

Alma Mater Studiorum Università di Bologna  
Archivio istituzionale della ricerca

Comparison of Low-, Mid-, and High-Frequency Raman Spectroscopy for an In Situ Kinetic Analysis of Lipid Polymorphic Transformations

This is the final peer-reviewed author's accepted manuscript (postprint) of the following publication:

*Published Version:*

Pasquarella C., Bertoni S., Passerini N., Boyd B.J., Bērziņš K. (2023). Comparison of Low-, Mid-, and High-Frequency Raman Spectroscopy for an In Situ Kinetic Analysis of Lipid Polymorphic Transformations. CRYSTAL GROWTH & DESIGN, 23(11), 7947-7957 [10.1021/acs.cgd.3c00737].

*Availability:*

This version is available at: <https://hdl.handle.net/11585/951433> since: 2023-12-28

*Published:*

DOI: <http://doi.org/10.1021/acs.cgd.3c00737>

*Terms of use:*

Some rights reserved. The terms and conditions for the reuse of this version of the manuscript are specified in the publishing policy. For all terms of use and more information see the publisher's website.

This item was downloaded from IRIS Università di Bologna (<https://cris.unibo.it/>).  
When citing, please refer to the published version.

(Article begins on next page)

# Comparison of Low-, Mid- and High-Frequency Raman Spectroscopy for *In Situ* Kinetic Analysis of Lipid Polymorphic Transformations

Chiara Pasquarella<sup>a,b</sup>, Serena Bertoni<sup>b</sup>, Nadia Passerini<sup>b</sup>, Ben J. Boyd<sup>a,c\*</sup>, Kārlis Bērziņš<sup>a\*\*</sup>

<sup>a</sup>Department of Pharmacy, Faculty of Health and Medical Sciences, University of Copenhagen, Copenhagen 2100, Denmark

<sup>b</sup>Department of Pharmacy and Biotechnology, University of Bologna, Via S. Donato 19/2, 40127 Bologna, Italy

<sup>c</sup>Drug Delivery, Disposition and Dynamics, Monash Institute of Pharmaceutical Sciences, Parkville 3052, VIC Australia.

\*Co-corresponding author (ben.boyd@sund.ku.dk)

\*\*Corresponding author (karlis.berzins@sund.ku.dk)

## Abstract

The performance of selected spectral ranges in the low (10-150 cm<sup>-1</sup>), mid (1350-1500 cm<sup>-1</sup>) and high (i.e., C-H stretching; 2800-2950 cm<sup>-1</sup>) frequency domains of Raman spectroscopy was evaluated for the kinetic *in-situ* analysis of lipid polymorphic transformations. Tristearin was used as the primary model lipid and its spray congealed formulations containing 5% w/w isopropyl myristate (IM), oleic acid (OA) and ethyl oleate (EO) were used due to their ability to differently modulate the tristearin phase transformation from metastable  $\alpha$ -form to the stable  $\beta$ -form. Behaviour of bulk samples was interrogated under different isothermal conditions (35, 40, 45 and 50 °C) with Raman microscopy providing complimentary particulate level information for specific conditions, including dispersed state within aqueous environment. Overall, a clear rank-order was observed between the lipid additives (IM>EO>OA) for accelerating the conversion to  $\beta$ -form, best exemplified by the low-frequency Raman (LFR) domain. This spectral range also showed superior characteristics over the more commonly utilized mid-frequency and C-H stretching domains to detect faster onset times for the polymorphic transformations that was attributed to its intrinsic structural sensitivity.

## Introduction

With the advent of lipid-based formulations for poorly soluble drugs, and lipid nanoparticles for mRNA, there is growing interest in lipid excipients. However, lipids present challenges in manufacture and storage of lipid-based pharmaceutical products due to polymorphic transformations that can be highly dynamic in their nature and affect the physical appearance, release profile and, ultimately, the overall performance of the formulation.<sup>1</sup> Polymorphic forms of the same chemical compound can have different physico-chemical and biopharmaceutical properties (e.g., morphology, stability, dissolution and bioavailability) that can strongly affect the final product efficacy.<sup>2,3</sup>

Triacylglycerols (TAGs) are a major lipid source widely utilized for the manufacture of pharmaceuticals as well as beauty and food products. Natural fats composed by TAGs often show complex polymorphism as a consequence of differences in the packing of aliphatic carbon chains. Many factors influence how a TAG crystallizes from the melt, including composition, temperature, presence of additives, mechanical treatment (shear, stirring, etc.) among others.<sup>4</sup> For this reason, the development of a good understanding of the landscape of polymorphic forms and their dynamics is required to ensure an appropriate performance and shelf-life of products incorporating TAGs. Typically, characterization of these processes has relied upon the use of optical microscopy, X-ray powder diffraction (PXRD), differential scanning calorimetry (DSC), solid-state nuclear magnetic resonance (ssNMR) as well as vibrational spectroscopy encompassing infrared and Raman spectroscopy.<sup>5</sup> The latter, specifically, has been extensively utilized to investigate lipid-based analytes due to the non-destructive nature of the

measurements, fast data acquisition speeds as well as inherently strong polarizability of lipids that results in increased signal propensity of the Raman bands.<sup>6</sup>

The advent of ultra-narrowband filter technology has also enabled easier access to the low-frequency Raman (LFR) domain  $<300\text{ cm}^{-1}$  that probes intermolecular motions and can provide direct information on structural properties.<sup>7</sup> Although underutilized for the analysis of lipid samples,<sup>8,9</sup> this spectral region has shown capacity to detect subtle structural differences even between polytypes – polymorphic forms that differ only in one dimension and can appear identical for conventional methods such as PXRD or mid-frequency Raman spectroscopy ( $300\text{--}1800\text{ cm}^{-1}$ ).<sup>10</sup> Additionally, the typical signal enhancement of LFR domain as well as the ease of distinguishing crystalline and disordered states via the presence of sharp phonon modes or broad vibrational density of states (VDOS) features has been successfully exploited to probe fast dynamics of drug solubilization in the presence of milk lipids<sup>11,12</sup> and analyze large-scale structural rearrangements within lipid mesophases upon hydration.<sup>9</sup>

This study aimed to utilize different Raman spectral domains for the *in situ* kinetic analysis of lipid polymorphic phase transformations. Tristearin (SSS; Figure 1), a popular TAG was used as the primary model compound, with several lipid additives serving as crystallization modifiers (namely, isopropyl myristate, oleic acid and ethyl oleate). These additives were selected based on several factors: (i) their structural differences, (ii) their miscibility with molten tristearin that allows for them to be simply added to the lipid mixture in a melting-based processes, and (iii) the previously established rank-order ( $\text{IM} > \text{EO} \geq \text{OA}$ ) for accelerating the conversion of the tristearin metastable  $\alpha$ -form towards the stable  $\beta$ -form.<sup>13</sup> Overall, tristearin exhibits a complex solid-state form landscape with three main polymorphic forms –  $\alpha$ ,  $\beta'$  and  $\beta$  that share hexagonal, orthorhombic and triclinic packing of their alkyl chains, and exhibit progressively higher melting points at  $\sim 54$ ,  $64$ , and  $73\text{ }^{\circ}\text{C}$ , respectively.<sup>14</sup> Additionally, two configurations of the  $\beta'$ -phase have been suggested in the literature ( $\beta'_1$  and  $\beta'_2$ ) that are formed under specific temperature conditions above the melting point of the  $\alpha$ -form ( $\sim 54\text{ }^{\circ}\text{C}$ ).<sup>15,16</sup> Recently, similar nomenclature has been proposed for the stable  $\beta$ -form with the discovery of a phase with an increased melting temperature ( $\sim 76\text{ }^{\circ}\text{C}$ ) after a 2-year crystallization from acetone ( $\beta_2$ ).<sup>17</sup>

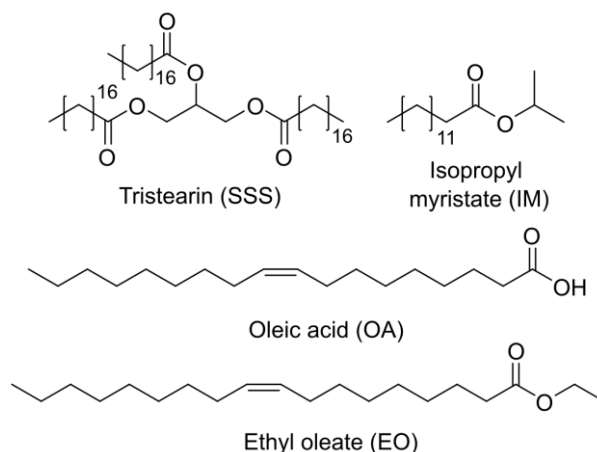


Figure 1. Molecular structures of tristearin, isopropyl myristate, oleic acid and ethyl oleate.

The monotropic relationship of this polymorphic behavior represents a challenge for the production of stable tristearin-based formulations via melt-based techniques. The cooling step typically results in the solidification of the metastable  $\alpha$ -form that can take different pathways towards the  $\beta$ -form in a broad range of time-scales depending of the ambient conditions (for example, it can take up to a year for the traces of the  $\beta$ -form to appear when stored at  $\sim 25\text{ }^{\circ}\text{C}$ ).<sup>13</sup> In the food industry, for products like butter and margarine,  $\alpha$  and  $\beta'$  are the desirable forms of TAGs, because of their texture and fluidity.<sup>18</sup> On the other hand, in pharmaceutical industry,  $\beta$ -form is usually desired to obtain stable lipid-based formulations as uncontrolled polymorphic transformations to more stable forms upon

processing and/or storage can alter important properties (such as changes in the API dissolution profile) of the final dosage form.

In this study, spray congealed microparticles with 5% w/w of liquid lipid additives were used to as an example of a melting-based, solvent-free manufacturing process for TAG formulations. This approach allowed the modulation of the kinetic behavior of the  $\alpha \rightarrow \beta$  transition within rational timescales that was investigated under different isothermal conditions (35, 40, 45 and 50 °C). Three specific Raman spectral regions were compared for their ability to reveal relevant information to these processes. The specific ranges representing MFR (1350-1500  $\text{cm}^{-1}$ ) and C-H stretching (2800-2950  $\text{cm}^{-1}$ ) domains were selected based on the data by Da Silva *et al.* that showed significant spectral differences between the polymorphs.<sup>14</sup> LFR spectroscopy has not been previously utilized for the solid-state analysis of TAGs. To retain a similar number of variables for multivariate chemometric analysis amongst all of the domains, a range of 10-150  $\text{cm}^{-1}$  was selected. Two different Raman experimental setups were utilized to investigate the phase behavior. A modular Raman system with free-space optics was used to interrogate bulk properties. Additionally, complementary particulate level information was accessed via Raman confocal microscopy that has been extensively utilized to characterize lipid vesicles from an optical and molecular point of view.<sup>19</sup> The kinetic modelling was facilitated by multivariate analytical tools including principal component analysis (PCA) and multivariate curve resolution (MCR).

Overall, each spectral range showed different propensity for distinguishing the polymorphic transformations of tristearin. Although the same trends were resolved by LFR, MFR and the C-H stretching domain with progressively faster transitions occurring at higher temperatures in bulk (concurrently affected by the presence of lipid additives following a rank order of IM>EO>OA), there were distinct differences in representation of different forms and their time-scales. For example, the high spectral similarities between  $\alpha$  and  $\beta'$  forms in the C-H stretching domain disallowed to separate their temporal contributions in kinetic modelling. These observations were complemented by Raman microscopy results with identical tendencies. The LFR region showed the best characteristics due to its structural sensitivity that were exemplified by the detection of unique features for the  $\beta$ -form (oppose to spectral shifts in MFR) and faster onset times for phase transitions (up to 5 min). These outcomes underline the possibility to obtain different information from specific spectral regions of a Raman spectrum and highlight the advantages of the LFR domain to characterize intricate solid-state transformations of lipid-based formulations.

## Experimental Section

**Materials.** Tristearin (Dynasan®118;  $\geq 99\%$ ) was kindly provided by IOI OLEO GmbH (Hamburg, Germany). Ethyl oleate (EO, tested according to Eur. Pharm.) and oleic acid (OA, tested according to Eur. Pharm.) were purchased from Carlo Erba Reagents (Milan, Italy). Isopropyl myristate (IM;  $\geq 95\%$ ) was obtained from Fluka (Buchs, Switzerland). Tween 80 was purchased from Sigma-Aldrich (Søborg, Denmark).

**Preparation of tristearin microparticles.** Microparticles were produced via spray congealing as described elsewhere.<sup>13</sup> In short, a wide pneumatic nozzle was used - a two-fluid atomizer, based on compressed air and melted mixture, characterized by a wide (4.5 mm) orifice opening. In this configuration, the air crosses the fluid with an inclination of 45° and generates a uniform spray pattern composed by particles in the micron size range. A mixture of tristearin and 5% w/w of liquid lipid additives were melted at 5 °C above the melting point of  $\beta$ -tristearin (72-73 °C). The nozzle temperature and the atomization pressure were set at 5 °C above the highest melting point of the mixture and at 1.5 bar, respectively. Droplets solidified into the cooling chamber that was maintained at 25 °C. The solidified microparticles were collected from the bottom of the cooling chamber and stored at 25 °C.

**Preparation of tristearin reference solid-state forms.** The  $\beta$ -form was used directly from the commercial supplier, whereas the  $\alpha$ -form was prepared by heating ~20 mg of tristearin inside an aluminum pan (TA Instruments, New Castle, DE, USA) to 90 °C using A PE120 variable-temperature stage with a T95 system controller (Linkam Scientific Instruments Ltd, U.K.), holding the sample at

that temperature for 2 min and then cooling it to 20 °C with 20 °C/min. The  $\beta'$  polymorph was prepared using a slightly modified methodology described in the literature.<sup>14</sup> A differential scanning calorimeter (Q2000, TA Instruments, New Castle, DE, USA) was used to heat an aluminum pan (TA Instruments, New Castle, DE, USA) with 8 mg of tristearin to 90 °C at 50 °C min<sup>-1</sup>. After equilibration, the sample was cooled to 57 °C at the same rate and then held isothermally for 30 min – this step was modified from the original methodology as the suggested annealing time of 100 min promoted formation of the  $\beta$  polymorph. The identity of all the procured phases was cross-referenced to the data by Da Silva *et al.* where detailed characterization of  $\alpha$ ,  $\beta'$  and  $\beta$  forms was carried out using conventional Raman spectroscopy, PXRD and DSC.<sup>14</sup>

**Raman spectroscopy.** THz-Raman® system (Ondax Inc., Monrovia, CA, USA) was used for collecting the Raman data with an excitation source from a 300 mW 785 nm laser module (Ondax Inc., Monrovia, CA, USA). The backscattered light (180° geometry) was collected using a free space optics accessory. The collected light was filtered through a set of volume Bragg gratings (Ondax Inc., Monrovia, CA, USA), and focused into spectrograph (Ondax Inc., Monrovia, CA, USA) via a fiber-optic cable. The light was then dispersed onto a CCD detector (Andor iVac 316, Oxford Instruments, Abingdon, UK). Spectra were collected over the spectral window -870 to 3200 cm<sup>-1</sup> with 4-6 cm<sup>-1</sup> resolution. For a typical measurement each spectrum was averaged from 5 scans with an integration time of 0.5 s. The sample spot size was approximately 0.5-1 mm.

**Isothermal kinetic studies of tristearin polymorphic transformations.** Raman spectra for the isothermal measurements were collected using the same principal setup as described above (Figure 2). A PE120 variable-temperature stage with a T95 system controller (Linkam Scientific Instruments Ltd, U.K.) was used for mounting the sample that was placed inside an aluminum pan (TA Instruments, New Castle, DE, USA). Initially, each tightly packed sample (~20 mg), was heated to 90 °C, held for 2 min at that temperature and then cooled to 20 °C with 20 °C/min and held at that temperature for 5 min to ensure sufficient time to reach thermal equilibrium. This step allowed to reliably procure tristearin in the  $\alpha$ -form. Afterwards, samples were heated to a selected temperature (35, 40, 45 or 50 °C) with a heating rate of 20 °C/min, and held at that temperature for an hour. For the kinetic analysis, only the triplicate data collected at the isothermal conditions was used. Each spectrum was comprised of five co-added scans with an integration time of 0.5 s for each scan.

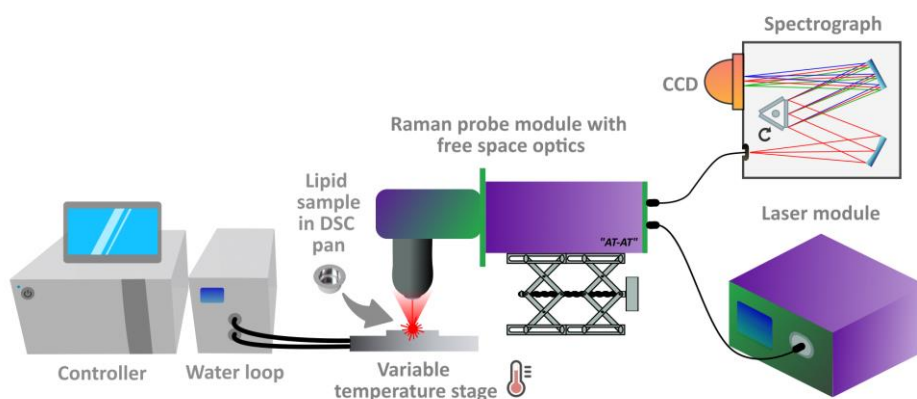


Figure 2. Schematic for the *in-situ* LFR instrumental configuration used to collect data during the isothermal polymorphic transformations of tristearin.

**Raman microscopy.** An Alpha 300R confocal Raman microscope (WITec, Ulm, Germany) equipped with a TrueSurface module (TSM) and RayShield coupler that enable topographic Raman imaging and access to the LFR spectral domain, respectively was used to interrogate particulate information of tristearin samples under different conditions. For imaging of tristearin at dry yet elevated temperature conditions (i.e., 50 °C), measurements were carried out with the 532 nm laser and 20x objective (~550 nm spotsize) in a mapping arrangement (100 x 100  $\mu$ m; 4  $\mu$ m step size) with a laser power of 40 mW, spectral range from -445 to 3935 cm<sup>-1</sup> and integration time of 1 second. TSM settings

were set to 10% maximum shift, 5% minimum signal, P-gain value of 3 and I-gain value of 0. Spectra were obtained using Project 6.1 software (WITec, Ulm, Germany) and analyzed with TrueComponent® analysis tool within the same software environment after preprocessing (see below). The same setup as for isothermal LFR studies was utilized with PE120 variable-temperature stage housing the sample, where a well packed sample (~30 mg) was heated to 90 °C and then cooled to 20 °C with 20 °C/min. After an equilibration period of 5 min it was heated until 50 °C with the fastest rate of 20 °C/min. Acquisition started at the beginning of the isothermal period and each Raman image dataset was recorded at ~14 minute intervals up to 3 hours.

The same principal experimental configuration was also used to investigate the phase behavior of dispersed tristearin and 5% w/w oleic acid particles in aqueous media containing Tween 80 (7.5% w/w). Microparticle dispersions (20 mg/mL) were prepared using an Eppendorf thermomixer, where the samples (1 mL) were shaken at 2000 rpm whilst maintaining 90 °C for 3 hours. Afterwards, flat glass capillaries were quickly filled, glue-sealed and briefly placed at -20 °C to promote fast formation of  $\alpha$ -phase. The analysis of samples was carried out immediately after their preparation. Considering the temperature-induced movement of particles in the medium, each spectrum was acquired after the adjustment of the focus (and position, if necessary) on a single particle, and was comprised of 10 co-added scans with an integration time of 0.5 s for each scan.

**Data pre-processing.** Raman spectra from THz-Raman® system were first pre-processed using Ondax OSX 1.2.16 software (Ondax Inc., Monrovia, CA, USA) to remove cosmic ray spikes ( $\leq 3$  pixel wide). Varied baseline corrections were applied on the different spectral domains individually using the spectroscopy module in Orange Data Mining 3.32.0 (University of Ljubljana, Ljubljana, Slovenia) software package.<sup>20</sup> For the low-frequency Raman (LFR) region (-300 to 300  $\text{cm}^{-1}$ ), a linear baseline correction was applied. However, due to the curved nature of the selected mid-frequency Raman (MFR) region (1350 to 1500  $\text{cm}^{-1}$ ) and C-H stretching domain (2800 to 2950  $\text{cm}^{-1}$ ), a rubberband baseline correction was required. Scale and scattering variation were also amended for each spectral region using standard normal variate (SNV) transformation in the same software. However, while for the MFR and C-H stretching domain data it was carried out over the same spectral range as the rubberband correction, only a limited window (10 to 150  $\text{cm}^{-1}$ ) was used for the LFR domain.

The spectra obtained from Raman microscopy were pre-processed using the same software as per data collection; Project 6.1 software (WITec, Ulm, Germany). Each spectrum was divided into three regions of interest: LFR (14 to 210  $\text{cm}^{-1}$ ), MFR (1350 to 1500  $\text{cm}^{-1}$ ) and C-H stretching domain (2700 to 3000  $\text{cm}^{-1}$ ). The cosmic rays were removed using the cosmic ray removal (CRR) tool (filter size of 3 and dynamic factor of 8), followed by a baseline correction using the shape background subtraction method (filter size of 300). TrueComponent® analysis was conducted for each spectral range individually. The generated Raman maps were presented using the same color scale to enable a direct temporal comparison between different polymorphs.

**Principal component analysis (PCA).** PCA was carried out on pre-processed and appropriately sorted Raman data (i.e., triplicate isothermal kinetic dataset, dataset comprised of initial spectra of all kinetic samples at different temperatures or Raman microscopy data from monitoring solid-state transformations of individual particles within aqueous media) in Orange Data Mining 3.32.0 (University of Ljubljana, Ljubljana, Slovenia) software environment using default settings.<sup>20</sup>

**Multivariate curve resolution (MCR).** The MCR-ALS GUI 2.0 package<sup>21</sup> was used in the MATLAB r2022b software environment (Mathworks Inc., MA, USA) in order to analyze the bulk isothermal kinetic data collected at different temperatures (detailed above). A mixture of preliminary PCA and singular value decomposition (SVD) results was used to denote the number of components for the models that were initially calculated using replicate data ( $n = 3$ ) at different conditions. In instances where similar tendencies were observed, a cumulative data set (where applicable; Figure 3) was also analyzed to construct a more global MCR model. Reference data for  $\alpha$ ,  $\beta'$  and  $\beta$  forms were used for the initial guesses of spectral profiles of the components for the pre-processed Raman data sets. The MCR models were calculated using non-negativity (concentrations and spectra of the components

must be positive) and closure (mass balance in the kinetic process) constraints with at least 1000 alternating least squares (ALS) iterations and convergence criteria of 0.01.

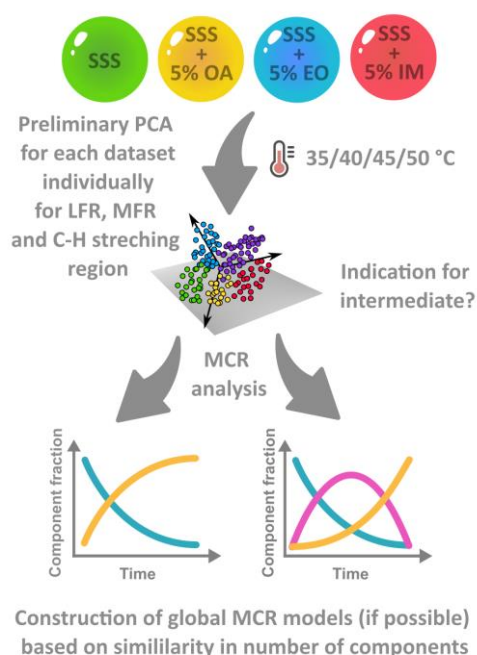


Figure 3. Flow chart of chemometric analysis for tristearin isothermal kinetic data monitored at different temperatures.

## Results and Discussion

**Exploratory analysis.** For comprehensive analysis of tristearin polymorphic phase transformations, it was important to first establish understanding of the Raman features for each of the tristearin solid-state forms. Figure 4 shows a comparison between three key spectral areas representing LFR, MFR and C-H stretching domains that were investigated in detail for  $\alpha$ ,  $\beta'$  and  $\beta$  configurations. No information on LFR (Figure 4a) features have been previously reported in the literature, where  $\alpha$ -form displays a broad VDOS feature with three apparent maxima at 14, 58 and 113  $\text{cm}^{-1}$ . Similarly,  $\beta'$ -form exhibits a limited number of distinct features at 14, 27, 62, 110 and 142  $\text{cm}^{-1}$  with a larger scattering propensity biased towards the quasi-elastic Raman domain  $<30 \text{ cm}^{-1}$ . On the other hand,  $\beta$ -form encompasses a number of well-defined peaks with a particularly unique feature at 29  $\text{cm}^{-1}$ . The observed higher spectral similarity between  $\alpha$  and  $\beta'$  forms can be rationalized with results from other structural characterization techniques. For example, both of these solid-state configurations are reported to exhibit similar PXRD patterns, indicating a stronger link between their structural attributes when compared to  $\beta$  phase.<sup>14</sup> Although aforementioned LFR bands can be associated with intermolecular vibrational modes (i.e., phonon or lattice vibrations), their true origin could only be interrogated using periodic boundary theoretical calculations<sup>22</sup> that were outside the scope of this study. In the selected MFR domain (1350-1500  $\text{cm}^{-1}$ ; Figure 4b), the observed spectral signatures were in agreement with those reported by Bresson *et al.*<sup>23</sup> and Da Silva *et al.*<sup>14</sup> All of the solid-state forms have fairly similar bands in the MFR range with most differences originating from the gradual blueshift of the  $\delta_s(\text{CH}_2)$  scissoring peak at 1438, 1442 and 1444  $\text{cm}^{-1}$ , and  $\delta_a(\text{CH}_2)$  asymmetric bending peak at  $\sim 1460.5$ , 1462 and 1466  $\text{cm}^{-1}$  for  $\alpha$ ,  $\beta'$  and  $\beta$ -form, respectively. It is important to note that  $\beta'$ -form encompasses some additional features at  $\sim 1413$  and 1422  $\text{cm}^{-1}$  that have been previously associated with  $\rho(\text{CH}_2)$  rocking vibrations.<sup>14</sup> The C-H stretching region (Figure 4c) was the least advantageous for distinguishing the polymorphs. Here, the subtle differences are related to the presence of a weak band at 2863  $\text{cm}^{-1}$  for  $\beta$ -form that has been associated with  $\nu_s(\text{CH}_3)$  symmetric stretching mode.<sup>23</sup> Other bands at 2847.5, 2883 and 2935  $\text{cm}^{-1}$  have been assigned to  $\nu_s(\text{CH}_2)$  symmetric stretching and  $\nu_s(\text{CH}_3)$  symmetric and  $\nu_a(\text{CH}_2)$  asymmetric stretching, respectively.<sup>14, 23</sup>

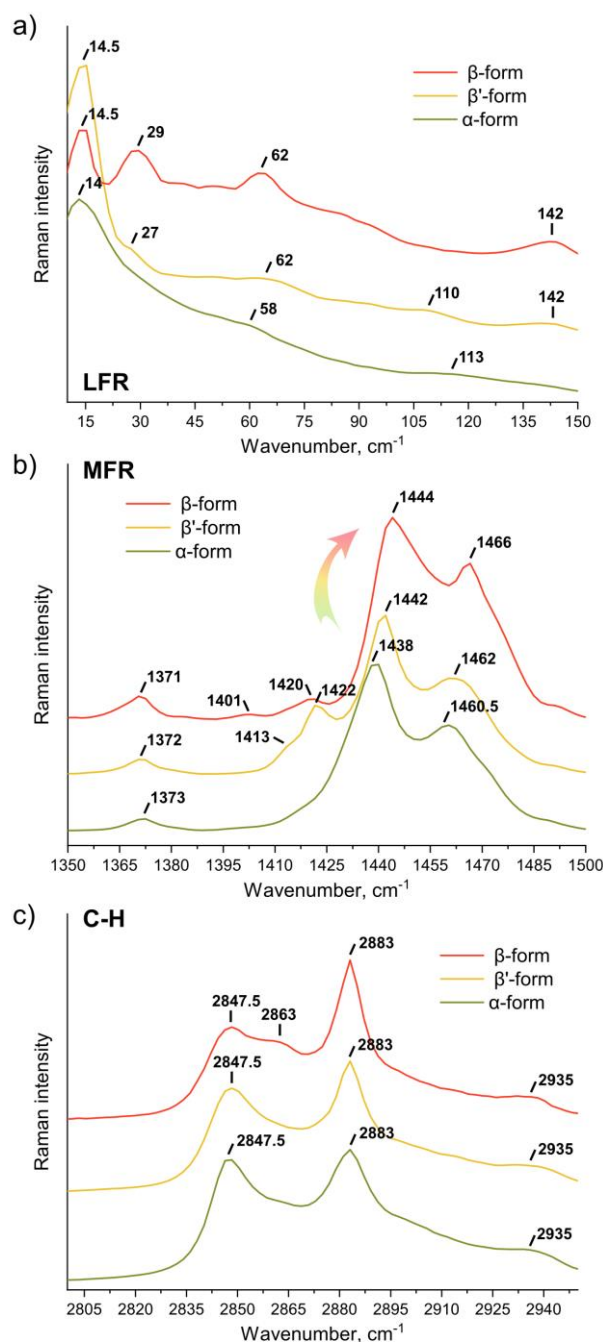


Figure 4. (a) Low-frequency Raman (LFR), (b) mid-frequency Raman (MFR) and (c) C-H stretching domain spectra examples of  $\alpha$ ,  $\beta'$  and  $\beta$ -form.

The isothermal conditions (35 to 50  $^{\circ}\text{C}$ ) for the kinetic analysis were selected based on the results from the previous study, where the effect of a range of lipid-based additives on tristearin solid-state form transformations was investigated in detail using thermal methods.<sup>13</sup> Figure 5 illustrates key findings from the analysis of pure tristearin samples that helped to establish a baseline understanding of the process. It is important to note that preliminary PCA of the initial Raman spectra (particularly LFR and MFR domain) of the procured  $\alpha$ -form brought to different isothermal conditions revealed certain important differences. For example, a clear differentiation of tristearin samples in LFR data were observed with the PC1 *versus* PC2 plot (Figure S1a) that showed a separation from the other samples (i.e., containing 5% w/w OA, EO and IM as lipid additives) depicted in the negative PC1 space. Additionally, almost linear, temperature-dependent evolution of score values was noted upwards in the



PC2 space for all the samples that trended towards higher temperature. Similar, albeit less distinct tendencies were also observed for the MFR data with the clustered tristearin samples projected in the negative PC1 space and the temperature dependence regressing with PC2 score values (Figure S2). On the other hand, the C-H stretching region showed a poor correlation to the metadata (i.e., sample composition and/or temperature condition; Figure S3). These observations had the following implications: (i) the resolved VDOS shifts in the PC1 loadings plot of LFR data (Figure S1b) may exemplify the sensitivity of LFR to better detect spectral contributions from lipid additives even at 5% w/w; (ii) the strong Raman signal temperature dependence of TAGs need to be considered when selecting a strategy for isothermal kinetic data analysis, where typically used global or cumulative chemometric models encompassing data from multiple samples/temperatures<sup>24</sup> would not be optimal or even viable due to significant spectral variance originating outside the realm of phase transformations. In this instance, the kinetic data analysis was segregated based on the composition (i.e., samples with or without lipid additives) as well as temperature.

At lower temperatures (i.e., 35 and 40 °C) only very minimal spectral changes were observed for pure tristearin samples (Figure S4), indicating almost no transformation of  $\alpha$ -form, whereas further increase in temperature accelerated the process. This is best seen in the left panel of Figure 5, where distinct spectral changes of each Raman domain of interest can be observed for the recorded transformation at 50 °C. Visually, the evolution of spectra indicated formation of  $\beta$ -form, however, to elucidate the presence of potential intermediate(s), several exploratory analysis steps were carried out (here and elsewhere) prior to semi-quantitative multivariate curve resolution (MCR) modeling in which the original data is expressed through a bilinear model of meaningful contributions of pure components. First, each triplicate data set was analyzed with PCA, where inverse temporal change of PC score values would indicate a presence of an intermediate. These observations were cross-checked on a larger scale among combined datasets (where applicable according to the data analysis strategy) using a singular value decomposition (SVD) relative to different number of components tested for the model. In all instances, either two or three components were found to be optimal for modelling the kinetic behavior of the  $\alpha \rightarrow \beta$  phase transformation, depending on the Raman spectral range used. In contrast to LFR and MFR, MCR models utilizing C-H stretching domain were incapable of distinguishing  $\beta'$  signature (i.e., procuring physically meaningful three or more components) and, hence, its contributions likely due to its intrinsic spectral similarity to  $\alpha$ -form (Figure 4c) in this Raman domain.

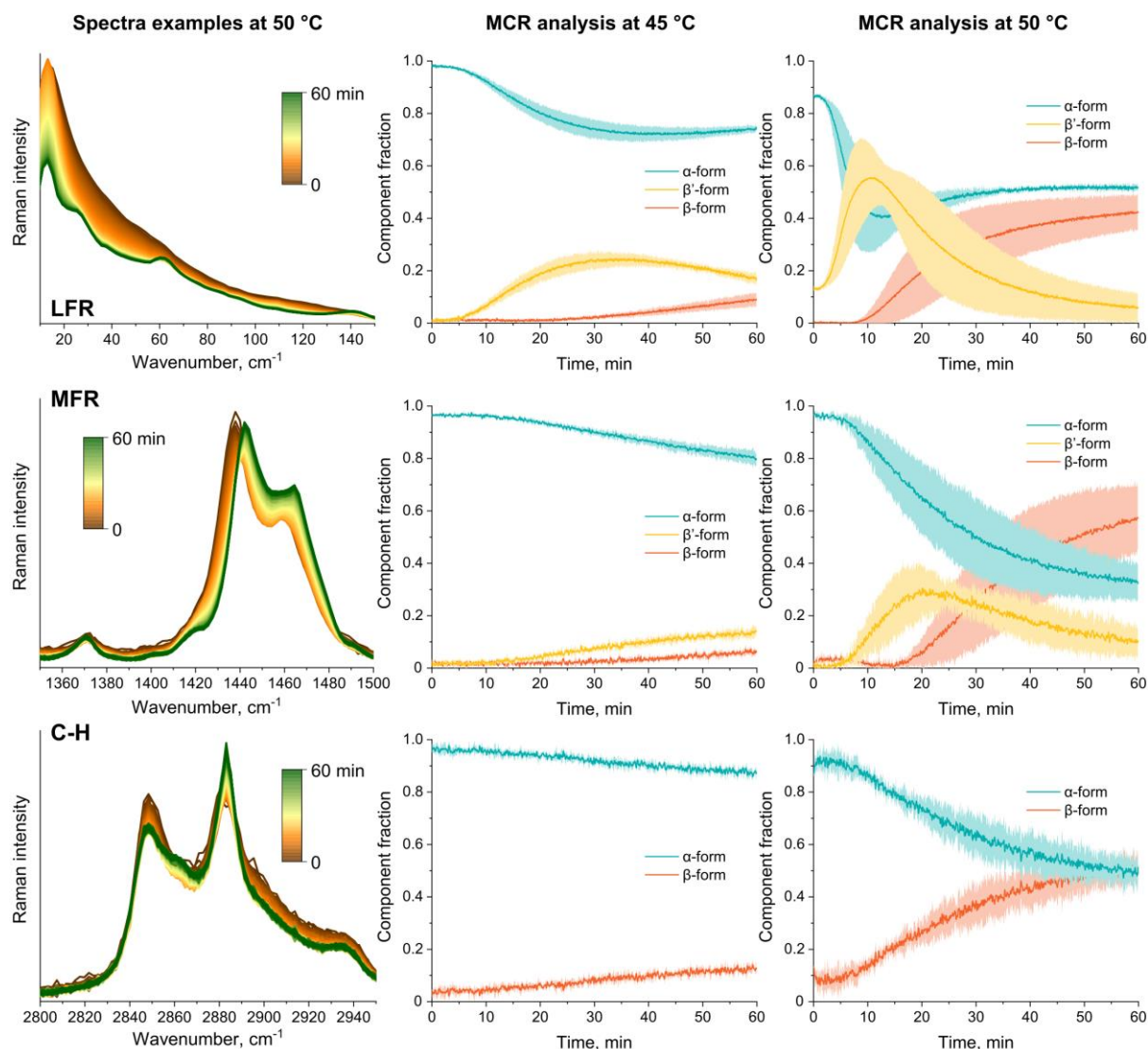


Figure 5. Representative Raman spectra in the LFR, MFR and C-H stretching domain during the solid-state changes of tristearin at 50 °C (left side panels), and MCR mean component concentrations with standard deviations between replicate runs (shaded;  $n = 3$ ) at 45 °C (middle panels) and 50 °C (right side panels). The resolved component spectral profiles of respective models are presented in Figure S5 and S6.

The MCR results of tristearin kinetic data at 45 and 50 °C (Figure 5 middle and right side panels, respectively) showed significant differences not only relative to the temperature conditions, but also the spectral domains used for the analysis. At 45 °C, only a modest transition of  $\alpha$ -form was resolved rational to observations made at lower temperatures (Figure S4). Interestingly, LFR predicted the onset formation of  $\beta'$  to be  $\sim 5$  min faster than MFR that could be related to its superior sensitivity to probe changes in long-range order, which expectedly take place during the rearrangement of alkyl chain packing from hexagonal ( $\alpha$ -form) to orthorhombic ( $\beta'$ -form). Similar advantages of LFR domain have been noted for investigating other types of solid-state transformations such as dehydration, where, for example, formation of anhydrous piroxicam from its monohydrate phase was detected on different timescales (i.e., up to several minutes) even at highly elevated temperatures ( $>90$  °C) where the overall transition occurs swiftly.<sup>25</sup> Analogous trends were also observed at 50 °C, where the transitions were more rapid that, in return, also promoted significant formation of  $\beta$ -form. Despite the variability in model components, the predicted composition between  $\alpha$  and  $\beta$  remained comparable regardless of the utilized spectral domain for the MCR analysis with endpoints indicating only partial conversion within

60 minutes. These results were in agreement with Raman microscopy data collected for tristearin at the same conditions (modelled using inputs from references; Figure S7), where only partial formation of  $\beta$ -form was also observed (Figure S8). It is important to note that although the data collection settings were tuned to maximize signal quality, chemometric models that encompassed  $\beta'$ -form reference data (or were built using three or more software-estimated components) were found to be invalid. This could be a consequence of a number of factors such as the spatial presence of  $\beta'$ -form below the limit of detection or spectral resolution hindrance (for LFR, it could also result from the inferior efficiency of the Raman microscope notch filter when compared to the free-space optics system that limits the reliably accessible spectral range). Nevertheless, the tendencies remained similar when only two components were considered ( $\alpha$  and  $\beta$  form), where significant changes occurred within ~42 minutes (concurrent within optical images and Raman maps). Interestingly, similar composition was retained throughout the experiment (~3 hours) with only small changes that may indicate that complete conversion requires melting of the  $\alpha$ -form (~54 °C) to better facilitate the rearrangement of alkyl chains.

**Isothermal analysis of tristearin polymorphic transformations in the presence of lipid additives.** Herein, three different liquid lipids (OA, EO and IM) were selected as the polymorphic modifiers that have previously shown different affinity for accelerating the formation of the tristearin stable  $\beta$ -form.<sup>13</sup> The isothermal kinetic data were collected at 35, 40, 45 and 50 °C for each of the formulations with the corresponding MCR concentration profiles for LFR, MFR and C-H stretching domain data presented in Figure 6, Figure S9 and Figure S10, respectively. The overall results showed several clear differences to the tristearin-only samples. First, the changes in solid-state form were greatly accelerated, best illustrated in the detectable changes even at 35 °C. These conditions (Figure 6, top-side panels) were also best to exemplify the rank order of IM>EO>OA for escalating the process via the gradual reduction in the modeled induction times. Interestingly, both MCR models utilizing LFR and MFR data independently indicated a higher temporal  $\beta$  to  $\beta'$  form ratio at 35 °C when compared to tristearin-only that first displayed detectable solid-state changes (i.e., at 45 °C). This may indicate the ability for the lipid additives to not only modulate the kinetic rate but also the mechanism of the process.

As expected, faster  $\alpha \rightarrow \beta' \rightarrow \beta$  conversion was observed at higher temperatures with a timing that was progressively reduced with formulations containing OA, EO and IM, likely promoting chain mobility that is advantageous for conformational changes. A similar explanation has been presented for tristearin  $\alpha \rightarrow \beta$  transformation in the presence of various emulsifiers.<sup>26</sup> Considering the different degrees of freedom between the alkyl chains of unsaturated and saturated fats, it is expected that IM would cause higher (localized) disorder in the solidified tristearin matrix that, in return, may provide lesser energy barrier for the transitions to  $\beta'$  and  $\beta$ -form to occur. This also correlates with the observed differences in the LFR VDOS shape from the PCA of procured tristearin  $\alpha$ -form with or without the presence of additives (Figure S1). The mechanistic differences between OA and EO for inducing similar effects may be further related to their physicochemical properties, particularly the disparities in their melting points (13-14 °C and -32 °C, respectively), and hydrogen bonding capacity influencing lipid-lipid interactions. Although the resolved MCR component spectral profiles (Figures S11 to S14) were in close agreement to reference data (Figure 4), the differences observed in LFR profiles underline the temperature influence on the organization of molecules and its potential consequences on long-range order arrangements. Similar to previous analysis, differences in induction times between spectral domains were also noted, albeit these were more difficult to compare at higher temperatures ( $\geq 45$  °C). In part, this was due to the resolved contributions of  $\beta'$  in MCR profiles from the LFR data, indicating a mixture between  $\alpha$  and  $\beta'$  forms at the start of the kinetic analysis at elevated temperature conditions. There were also differences between the form ratio endpoints that may elude to the limitations of the semi-quantitative nature of the MCR analysis. Nevertheless, all of the models showed a transformation trend that was not fully complete within 60 minutes and reached a certain plateau (more distinct at higher temperatures).

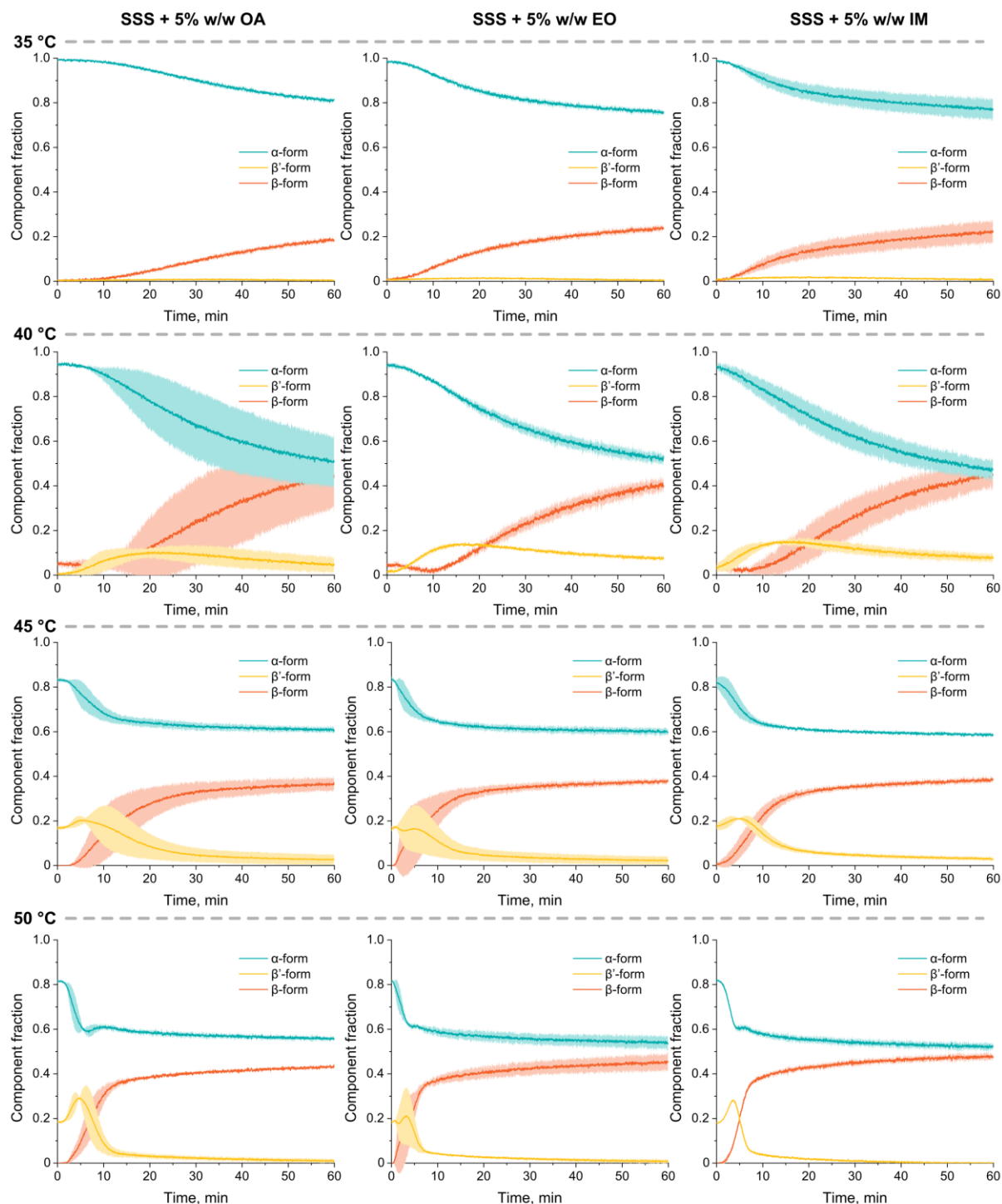


Figure 6. MCR analysis of LFR data with mean component concentrations with standard deviations between replicate runs (shaded;  $n = 3$ ) for tristearin samples with different additives at 5% w/w concentration: oleic acid (OA; left-side panels), ethyl oleate (EO; middle panels) and isopropyl myristate (IM, right-side panels). The resolved component spectral profiles of respective models for each temperature (35, 40, 45 and 50 °C) are presented in Figure S11, S12, S13 and S14.

From a formulation perspective, it is also important to understand the solid-state transformations of such particles within an aqueous environment, considering their ultimate purpose to serve as a drug delivery vehicle. As such, tristearin and 5% w/w OA microparticles were selected among the samples to be investigated by dispersing them inside a flat glass capillary, performing a heat/cool cycle to predominantly obtain  $\alpha$ -phase, and analyzing their solid-state behavior using Raman microscopy under

the same isothermal conditions as utilized before. Figure 7 highlights the main results of this analysis with a series of optical images, MFR spectra examples at 35 °C and PCA summary. Although it was difficult to distinguish any visual differences between the particles (Figure 7a), temporal evolution of the spectral data, especially in the MFR domain (Figure 7b), revealed noticeable changes – primarily with the peak shift from 1438 to 1443  $\text{cm}^{-1}$  that was associated with the gradual phase transformation to  $\beta$ -form. PCA allowed to further interrogate the temperature-induced differences of this process. In this instance, PC1 explained 85% of spectral variance with the  $\delta_s(\text{CH}_2)$  scissoring peak shift contributions split between the negative and positive PC space within the loadings plot (Figure 7d). The sigmoidal nature (with intrinsic induction time) and gradual change towards the positive PC space of PC1 score values (Figure 7c) allowed to compare the relative time-scales of the conversion that became more rapid  $\geq 45$  °C. It is interesting to note, however, that transformation at 35 °C appeared to be slower when compared to one at dry conditions (Figure 6; top left panel). This could be a result of multiple factors, namely the limited heat transfer due to aqueous matrix as well as the intrinsic high hydrophobicity of lipid particulates that may prevent water to mediate the phase transformation. A similar analysis using LFR and C-H stretching domain data was less clear (Figure S15 and S16) that was attributed to the technical limitations and structural sensitivity issues, respectively. More specifically, the limited efficacy of the accessible LFR spectral window from the microscope in combination with VDOS contributions from the water, and small differentiation between the tristearin solid-state configurations in the C-H domain were assumed to be the likely causes for this hindrance.

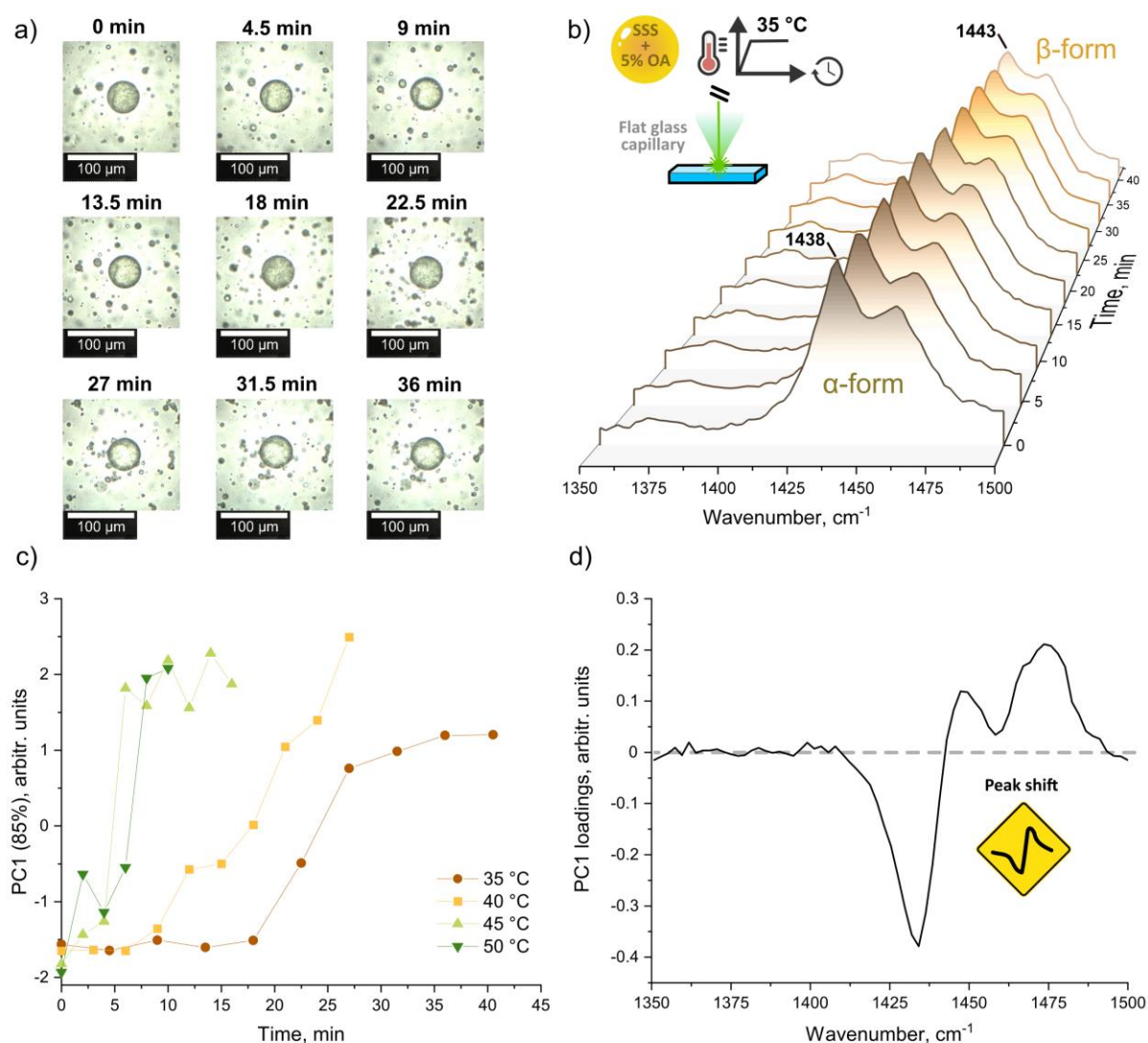


Figure 7. (a) Representative optical images and (b) MFR spectra of suspended tristearin microparticles containing 5% w/w oleic acid that were sealed inside a flat glass capillary (aqueous environment) and monitored at 35 °C; comparison of PCA of MFR spectral data collected at different temperatures (35, 40, 45 and 50 °C) for individual microparticles with (c) PC1 temporal score values plot and (d) loadings plot. The lines are drawn to assist in visualizing the trends.

**Significance.** Raman spectroscopy has been established as a powerful tool in various research areas and applications.<sup>27</sup> Our results further exemplify this by highlighting how a modern interpretation of the technique via inclusion of the LFR spectral domain can aid *in situ* monitoring of lipid polymorphic transformations. In this scenario, the typical advantages of Raman spectroscopy such as fast data acquisition speed and non-destructive nature of the measurements can be amplified with superior structural sensitivity to many conventional solid-state analytical techniques.<sup>7</sup> Here, these characteristics were best highlighted by the resolved temporal differences in the formation of  $\beta'$  and  $\beta$ -form among the tristearin formulations containing different additives. Such information can not only be used for direct comparison purposes, but it can also help to extrapolate tendencies at other (temperature) conditions with practical relevance. We expect that further developments in LFR-tuned optical filters and their continued adaption in commercial Raman instruments will propel the inclusion of LFR spectroscopy within a standard analytical framework for lipid-based material research and commercial manufacture.

## Conclusion

Different Raman spectral ranges representing LFR, MFR and C-H stretching domains were compared for the *in situ* kinetic analysis of transformations in lipid solid-state form. Spray-congealed tristearin microparticles, containing 5% w/w of lipid liquid additives (OA, EO and IM), were used as the primary model systems, and their phase behavior (i.e.,  $\alpha \rightarrow \beta' \rightarrow \beta$  conversion) was compared among the formulations as well as to control tristearin samples under different isothermal conditions (35 to 50 °C). The kinetic analysis was facilitated by the use of chemometric methods including PCA and MCR. A clear rank order was established between the Raman spectral domains (LFR > MFR > C-H stretching domain) for resolving the temporal solid-state form changes of interest. The C-H stretching domain was least able to distinguish the intermediate  $\beta'$ -form. The efficacy of LFR and MFR domains was more similar, although LFR was superior in detecting faster onset times (up to 5 min) for the polymorphic transformations. Additionally, LFR offered better spectral characteristics for distinguishing certain solid-state configurations, namely  $\beta$ -form (oppose to spectral shifts in MFR, detection of which can be compromised by spectral resolution). These findings suggest a potential application of LFR spectroscopy as a solid-state monitoring tool within the pharmaceutical, food and cosmeceutical sectors for lipid-based products.

## Associated content

### Supporting information

PCA of the initial LFR, MFR and C-H stretching domain data for various tristearin samples brought to different temperatures for isothermal kinetic analysis, representative Raman spectra of tristearin samples at the start and end of the measurements at 35 and 40 °C temperature, resolved component profiles of MCR analysis of at 45 and 50 °C, Raman microscopy reference data for tristearin  $\alpha$ ,  $\beta'$  and  $\beta$ -form, temporal evolution and comparison of Raman images constructed using LFR, MFR and C-H stretching domain for kinetic analysis of tristearin sample at 50 °C, MCR analysis of MFR and C-H stretching domain kinetic data for tristearin microparticle formulations containing 5% w/w OA, EO and IM, and PCA of LFR and C-H stretching domain data from Raman microscopy measurements of tristearin 5% w/w OA dispersed microparticles within aqueous environment that were monitored under different isothermal conditions (35, 40, 45 and 50 °C).



## Acknowledgment

The authors acknowledge the Novo Nordisk Foundation for supporting this work. Ben Boyd and Kārlis Bērziņš are supported by a Novo Nordisk Laureate Research Fellowship awarded to Ben Boyd.

## ORCID

Serena Bertoni 0000-0002-5534-0892

Nadia Passerini 0000-0002-3470-2700

Ben J. Boyd 0000-0001-5434-590X

Kārlis Bērziņš 0000-0001-6545-5522

## References

- (1) Nakmode, D.; Bhavana, V.; Thakor, P.; Madan, J.; Singh, P. K.; Singh, S. B.; Rosenholm, J. M.; Bansal, K. K.; Mehra, N. K. Fundamental Aspects of Lipid-Based Excipients in Lipid-Based Product Development. *Pharmaceutics* **2022**, *14* (4).
- (2) Jannin, V.; Rosiaux, Y.; Doucet, J. Exploring the possible relationship between the drug release of Compritol®-containing tablets and its polymorph forms using micro X-ray diffraction. *J. Control. Release* **2015**, *197*, 158-164.
- (3) Lopes, D. G.; Koutsamanis, I.; Becker, K.; Scheibelhofer, O.; Laggner, P.; Haack, D.; Stehr, M.; Zimmer, A.; Salar-Behzadi, S. Microphase separation in solid lipid dosage forms as the cause of drug release instability. *Int. J. Pharm.* **2017**, *517* (1), 403-412.
- (4) Bayés-García, L.; Patel, A. R.; Dewettinck, K.; Rousseau, D.; Sato, K.; Ueno, S. Lipid crystallization kinetics—roles of external factors influencing functionality of end products. *Current Opinion in Food Science* **2015**, *4*, 32-38.
- (5) Law, D.; Zhou, D. Solid-State Characterization and Techniques. In *Developing Solid Oral Dosage Forms (Second Edition)*, Qiu, Y., Chen, Y., Zhang, G. G. Z., Yu, L., Mantri, R. V. Eds.; Academic Press, 2017; pp 59-84.
- (6) Czamara, K.; Majzner, K.; Pacia, M. Z.; Kochan, K.; Kaczor, A.; Baranska, M. Raman spectroscopy of lipids: a review. *J. Raman Spectrosc.* **2015**, *46* (1), 4-20.
- (7) Bērziņš, K.; Fraser-Miller, S. J.; Gordon, K. C. Recent Advances in Low-Frequency Raman Spectroscopy for Pharmaceutical Applications. *Int. J. Pharm.* **2021**, *592*, 120034.
- (8) Leonov, D. V.; Dzuba, S. A.; Surovtsev, N. V. Normal vibrations of ternary DOPC/DPPC/cholesterol lipid bilayers by low-frequency Raman spectroscopy. *RSC Adv.* **2019**, *9* (59).
- (9) Krog, L. S.; Kirkensgaard, J. J. K.; Foderà, V.; Boyd, B. J.; Bērziņš, K. Application of Low-Frequency Raman Spectroscopy to Probe Dynamics of Lipid Mesophase Transformations upon Hydration. *J. Phys. Chem. B* **2023**, *127* (14), 3223-3230.
- (10) Iwata, K.; Karashima, M.; Ikeda, Y.; Inoue, M.; Fukami, T. Discrimination and quantification of sulfathiazole polytypes using low-frequency Raman spectroscopy. *CrystEngComm* **2018**, *20* (14), 1928-1934.
- (11) Salim, M.; Fraser-Miller, S. J.; Sutton, J. J.; Bērziņš, K.; Hawley, A.; Clulow, A. J.; Beilles, S.; Gordon, K. C.; Boyd, B. J. Application of Low-Frequency Raman Scattering Spectroscopy to Probe in Situ Drug Solubilization in Milk during Digestion. *J. Phys. Chem. Lett.* **2019**, *10* (9), 2258-2263.
- (12) Salim, M.; Fraser-Miller, S. J.; Bērziņš, K.; Sutton, J. J.; Ramirez, G.; Clulow, A. J.; Hawley, A.; Beilles, S.; Gordon, K. C.; Boyd, B. J. Low-Frequency Raman Scattering Spectroscopy as an Accessible Approach to Understand Drug Solubilization in Milk-Based Formulations during Digestion. *Mol. Pharmaceutics* **2020**, *17* (3), 885-899.
- (13) Bertoni, S.; Passerini, N.; Albertini, B. Liquid Lipids Act as Polymorphic Modifiers of Tristearin-Based Formulations Produced by Melting Technologies. *Pharmaceutics* **2021**, *13* (7).
- (14) Da Silva, E.; Bresson, S.; Rousseau, D. Characterization of the three major polymorphic forms and liquid state of tristearin by Raman spectroscopy. *Chem. Phys. Lipids* **2009**, *157* (2), 113-119.
- (15) Simpson, T. D.; Hagemann, J. W. Evidence of two  $\beta'$  phases in tristearin. *J. Am. Oil Chem. Soc.* **1982**, *59* (4), 169-171.
- (16) Oh, J. H.; McCurdy, A. R.; Clark, S.; Swanson, B. G. Characterization and Thermal Stability of Polymorphic Forms of Synthesized Tristearin. *J. Food Sci.* **2002**, *67* (8), 2911-2917.

- (17) Ghazani, S. M.; Marangoni, A. G. New Triclinic Polymorph of Tristearin. *Cryst. Growth Des.* **2023**, 23 (3), 1311-1317.
- (18) Ribeiro, A. P. B.; Masuchi, M. H.; Miyasaki, E. K.; Domingues, M. A. F.; Stroppa, V. L. Z.; de Oliveira, G. M.; Kieckbusch, T. G. Crystallization modifiers in lipid systems. *J. Food Sci. Technol.* **2015**, 52 (7), 3925-3946.
- (19) Fox, C. B.; Uibel, R. H.; Harris, J. M. Detecting Phase Transitions in Phosphatidylcholine Vesicles by Raman Microscopy and Self-Modeling Curve Resolution. *J. Phys. Chem. B* **2007**, 111 (39), 11428-11436.
- (20) Demsar, J.; Curk, T.; Erjavec, A.; Gorup, C.; Hocevar, T.; Milutinovic, M.; Mozina, M.; Polajnar, M.; Toplak, M.; Staric, A.; et al. Orange Data: Mining Toolbox in Python. *J. Mach. Learn. Res.* **2013**, 14, 2349-2353.
- (21) Jaumot, J.; de Juan, A.; Tauler, R. MCR-ALS GUI 2.0: New features and applications. *Chemometrics Intellig. Lab. Syst.* **2015**, 140, 1-12.
- (22) Bērziņš, K.; Sutton, J. J.; Fraser-Miller, S. J.; Rades, T.; Korter, T. M.; Gordon, K. C. Solving the Computational Puzzle: Toward a Pragmatic Pathway for Modeling Low-Energy Vibrational Modes of Pharmaceutical Crystals. *Cryst. Growth Des.* **2020**, 20 (10), 6947-6955.
- (23) Bresson, S.; Marssi, M. E.; Khelifa, B. Raman spectroscopy investigation of various saturated monoacid triglycerides. *Chem. Phys. Lipids* **2005**, 134 (2), 119-129.
- (24) Remoto, P. I. I. J. G.; Bērziņš, K.; Fraser-Miller, S. J.; Korter, T. M.; Rades, T.; Rantanen, J.; Gordon, K. C. Elucidating the Dehydration Mechanism of Nitrofurantoin Monohydrate II Using Low-Frequency Raman Spectroscopy. *Cryst. Growth Des.* **2022**, 22 (4), 2733-2741.
- (25) Robert, C.; Fraser-Miller, S. J.; Bērziņš, K.; Okeyo, P. O.; Rantanen, J.; Rades, T.; Gordon, K. C. Monitoring the Isothermal Dehydration of Crystalline Hydrates Using Low-Frequency Raman Spectroscopy. *Mol. Pharmaceutics* **2021**, 18 (3), 1264-1276.
- (26) Aronhime, J. S.; Sarig, S.; Garti, N. Mechanistic considerations of polymorphic transformations of tristearin in the presence of emulsifiers. *J. Am. Oil Chem. Soc.* **1987**, 64 (4), 529-533.
- (27) Paudel, A.; Rajjada, D.; Rantanen, J. Raman Spectroscopy in Pharmaceutical Product Design. *Adv. Drug Del. Rev.* **2015**, 89, 3-20.

For Table of Contents Use Only

## Synopsis

The performance of different spectral domains of Raman spectroscopy was evaluated for *in-situ* kinetic analysis of lipid polymorphic transformations.

